Title

Quantum Markov chain Monte Carlo with digital dissipative dynamics on quantum computers

Journal

Quantum Science and Technology, 7(2)

ISSN

2058-9565

Authors

Metcalf, Mekena
Stone, Emma
Klymko, Katherine
et al.

Publication Date

2022-04-01

DOI

10.1088/2058-9565/ac546a

Peer reviewed

Quantum Markov Chain Monte Carlo with Digital Dissipative Dynamics on Quantum Computers

Mekena Metcalf,[1,*] Emma Stone,[2] Katherine Klymko,[1] Alexander F. Kemper,[2] Mohan Sarovar,[3] and Wibe A. de Jong[1,†]

[1]*Computational Research Division, Lawrence Berkeley National Laboratory, Berkeley, CA 94720, USA*
[2]*Department of Physics, North Carolina State University, Raleigh, North Carolina 27695, USA*
[3]*Extreme-scale Data Science and Analytics, Sandia National Laboratories, Livermore, CA 94550, USA*

Modeling the dynamics of a quantum system connected to the environment is critical for advancing our understanding of complex quantum processes, as most quantum processes in nature are affected by an environment. Modeling a macroscopic environment on a quantum simulator may be achieved by coupling independent ancilla qubits that facilitate energy exchange in an appropriate manner with the system and mimic an environment. This approach requires a large, and possibly exponential number of ancillary degrees of freedom which is impractical. In contrast, we develop a digital quantum algorithm that simulates interaction with an environment using a small number of ancilla qubits. By combining periodic modulation of the ancilla energies, or spectral combing, with periodic reset operations, we are able to mimic interaction with a large environment and generate thermal states of interacting many-body systems. We evaluate the algorithm by simulating preparation of thermal states of the transverse Ising model. Our algorithm can also be viewed as a quantum Markov chain Monte Carlo (QMCMC) process that allows sampling of the Gibbs distribution of a multivariate model. To demonstrate this we evaluate the accuracy of sampling Gibbs distributions of simple probabilistic graphical models using the algorithm.

I. INTRODUCTION

Much of simulation science is built upon modeling a system interacting with an environment in order to capture complex dissipative and relaxation dynamics. In the context of quantum mechanical systems, there are open-quantum systems described by dynamical semi-groups generating completely positive trace preserving (CPTP) maps. These semi-groups are constructed from generators, similar to Hamiltonians for closed-quantum systems. Simulation of general physical systems described by these semi-group generators on quantum computers has a long history with growing interest in implementing both Markovian and non-Markovian dynamics on quantum computers [1–8]. We are particularly interested in developing Markovian semi-groups that yield a thermal state as the fixed point of evolution. Sampling from difficult distributions like a multivariate Gibbs distribution on quantum computers has been proposed using Metropolis sampling algorithms that reduce time complexity [9–13], variational algorithms that are possibly well-suited to near-term quantum computers but have a classical optimization overhead [14, 15], thermo-field double states [16, 17], and quantum imaginary time-evolution to implement the minimally entangled typical thermal state (METTS) [18, 19] sampling algorithm on quantum computers [20, 21]. Our approach is different, as we engineer a discretization of a dynamical semi-group with an approximate macroscopic, thermal environment that generates the thermal/Gibbs state at any temperature for general system Hamiltonians.

Thermal states can be prepared by modeling open-quantum systems if the system and environment are weakly coupled, if the dynamics are ergodic, and if environment is in a thermal state [22–24]. However, it is not straightforward to guarantee that these conditions are met by an environment that is engineered from ancilla degrees of freedom, and moreover, the number of required ancilla degrees of freedom could scale exponentially with the degrees of freedom in the system to be thermalized (since the number of energy eigenstates scales exponentially with degrees of freedom). We address these difficulties by adding time-dependence to the ancilla qubits that approximate the environment; modulating the energy of these ancilla qubits across the system energy spectrum in a suitable manner – a process termed *spectral combing*. This procedure allows us to engineer the necessary conditions for thermalization with a number of ancillae that does not need to scale exponentially with the system size. Our algorithm is a method to emulate quantum Markov chain Monte Carlo (QMCMC) methods [25] on quantum devices [10, 26], and thus provides a general route to sample from Boltzmann distributions corresponding to the stationary states of Markov chains. In the case that the eigenvalues of the Hamiltonian are non-degenerate and known, the algorithm reduces to the classical Markov chain mapped to a quantum Hamiltonian [9]. An important application will be the preparation of thermal, initial states to simulate chemical and molecular reaction pathways [27] in large systems (where the classical dynamics become prohibitively expensive) at arbitrary temperatures. Our algorithm is designed to obtain thermal distributions of statistical physics problems with great accuracy. We find our algorithm is able to obtain thermal distributions for system Hamiltonians with degenerate sub-spaces needed for arbitrary quantum systems. For concreteness, we focus on spin systems, however, the general approach can be used to thermalize any many-body system whose Hamiltonian can be encoded in a many-qubit Hamiltonian.

Spectral combing using auxiliary qubits that exchange energy with the principal qubits periodically in time has been proposed for digital and analog unitary evolution to obtain ground states and thermal states [28, 29]. Our approach in Ref [24] used spectral combing to engineer detailed balance conditions on analog quantum computers. By engineering

* mmetcalf@lbl.gov
† wadejong@lbl.gov

the detailed balance conditions we can obtain high-accuracy, approximate thermal distributions on quantum devices [23]. We extend our previous method to digital quantum computers, and devise an algorithm that mimics the interaction of a system with a finite temperature macroscopic bath using time-dependent ancilla qubits. Our algorithm is motivated by the three criteria needed – defined above – for the thermal state to be the unique fixed point of evolution [22]. We test the performance of our algorithm by numerically evaluating the fidelity between the steady-state solution and the genuine thermal distribution for a transverse field Ising model (TFIM) with both open and periodic boundary conditions, and by computing the error in computing the thermal magnetization in the transverse direction. We also evaluate the performance of the algorithm on the problem of sampling multivariate Gibbs distributions over binary random variables with constraints generated by Erdós Rényi random graphs.

II. THEORETICAL FOUNDATION

Modeling finite temperature physics of quantum systems requires defining a composite Hilbert space of a system and a bath $\mathcal{H} = \mathcal{H}_s \otimes \mathcal{H}_b$. The total Hamiltonian defines the system H_s, the bath H_b, and the interaction between them H_i,

$$H = H_s \otimes I + I \otimes H_b + H_i. \tag{1}$$

We can now express the time-evolution operator of the total Hamiltonian

$$\rho(t) = U(t)\rho(0)U^\dagger(t), \tag{2}$$

$$U(t) = e^{-iHt}, \tag{3}$$

where we set $\hbar = 1$.

If the system and bath are weakly coupled, $||H_i|| \ll ||H_b||$ and $||H_s||$, and the bath is fast relaxing, the influence of the system on the bath state is negligible and we can make the Born and Markov approximations. The norm, $||.||$ is the spectral norm with $||H|| = \sqrt{E_{max}(H^\dagger H)}$. Further, defining the state of the system and bath at $t = 0$ as an uncorrelated product state, $\rho(0) = \rho_s(0) \otimes \rho_b$, tracing out the bath degrees of freedom the state of the system at time t,

$$\rho_s(t) = \mathrm{Tr}_b \left(U(t,0) \left[\rho_s(0) \otimes \rho_b \right] U^\dagger(t,0) \right), \tag{4}$$

$$\equiv \mathcal{M}\rho_s(0) \tag{5}$$

defines a completely positive, trace preserving (CPTP) dynamical map $\mathcal{M}$ on the system. This dynamical map is what we aim to approximately implement on a quantum computer. Under the conditions that the system dynamics are ergodic and that the bath-induced transitions between system eigenstates satisfy detailed balance [22], the unique fixed point of evolution is the thermal state

$$\rho_s(t) = \rho_{th} = \frac{e^{-\beta H}}{\mathrm{Tr}\left(e^{-\beta H}\right)}, \tag{6}$$

where $\beta = 1/k_B T$, and T is the equilibrium temperature defined on the bath and we set $k_b = 1$. Note that ergodicity is a condition on the system dynamics, including the system-environment interaction. Therefore, it is a condition on H_s and H_i – see Refs [22–24]. We demonstrate how these conditions can be satisfied by engineering a bath consisting of locally coupled, time-dependent ancilla spins.

III. QUANTUM ALGORITHM

The algorithm weakly couples a collection of M periodically modulated, thermal ancilla qubits (which function as the "bath") to an arbitrary multi-qubit system Hamiltonian (H_s) encoded on N_s, "principal qubits", Fig. 1(a). The composite Hamiltonian is defined as,

$$H_b(t) = -\sum_{m=1}^{M} \frac{\Omega(t)}{2} \tau_z^m \tag{7}$$

$$H_i = \sum_{m=1}^{M} g_m \left(\sigma_x^{\lambda(m)} \otimes \tau_x^m \right) \tag{8}$$

$$H(t) = (H_s \otimes I_b) + (I_s \otimes H_b(t)) + H_i, \tag{9}$$

where τ_α^m $(\alpha = x, y, z)$ are the Pauli spin operators acting on ancilla m, and $\sigma_\alpha^{\lambda(m)}$ are spin operators for the principal qubit coupled to ancilla m, see Fig. 1(a). $\lambda(m)$ simply returns the index of the principal, system qubit that is coupled to ancilla qubit m. The number of ancilla qubits scales at most as the number of principal qubits, $M = \mathcal{O}(N_s)$, but can be smaller than N_s in many cases. The exact number of ancilla required is determined by the fact that combined, H_s and H_i must satisfy the ergodicity conditions specified in [24]. In the above Hamiltonian we have modeled the system-ancilla interaction through a $\sigma_x^{\lambda(m)} \otimes \tau_x^m$ interaction. This is not uniquely specified. This could be any other interaction that promotes energy exchange between the system and ancilla degrees of freedom, e.g., $\sigma_y^{\lambda(m)} \otimes \tau_y^m$. The important element is that the system portion of this interaction (e.g., $\sigma_x^{\lambda(m)}$) cannot commute with H_s. If this interaction shares a common eigenbasis with the system Hamiltonian, time-dependent energy exchange is inhibited, preventing transitions between all states. Lack of ergodicity, e.g., due to symmetry, can be circumvented by alternating between different coupling terms [30]. The function $\Omega(t) = \omega_m f(t)$ represents the time-dependent modulation of the bath qubits, and sweeps across the system spectrum using a periodic function $f(t)$ with period T_{cycle} with an amplitude set by an estimate of the system Hamiltonian spectral width, $\omega_m \approx |E_{max} - E_{min}|$. Periodically modulating the energy of the *independent* ancilla spins enables an exchange of energy with different system frequency transitions at different times, see Fig. 1(b). Finally, while not necessary, in the following we will assume that the system-ancilla coupling, g_m, is the same for all m for simplicity.

Our approach in the following will be to approximate the above continuous evolution via a discrete Trotter evolution

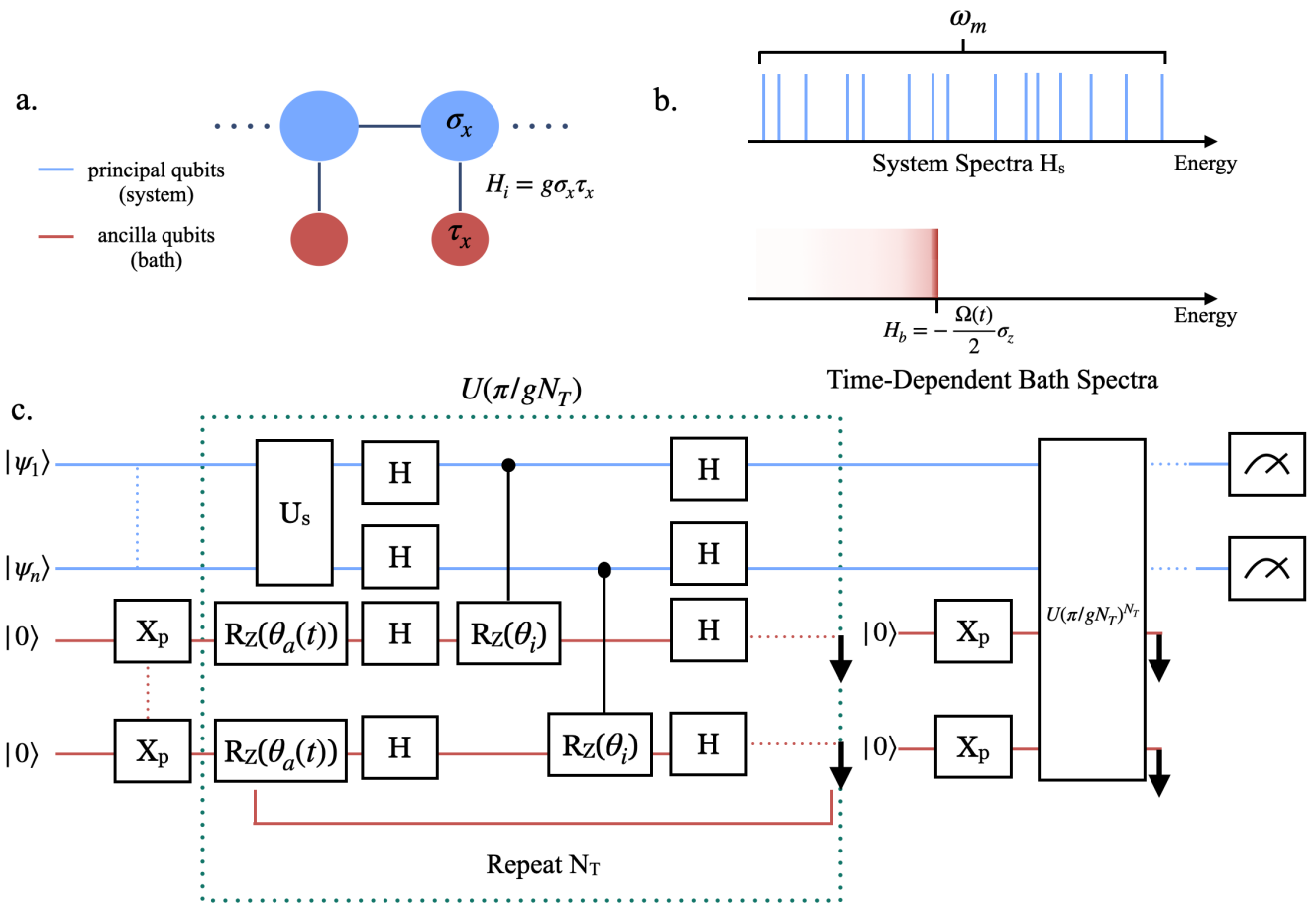

Figure 1. a) Principal qubits (blue) locally connected to ancilla qubits (red). b) Time-dependent ancilla frequency combs the system energy spectra and resonantly exchanges energy with different energy transitions in the system at different times c) Quantum circuit to implement the interaction cycle dynamical map in Eq. 14 for arbitrary system size. $U_s = e^{-iH_s\pi/gN_T}$ and $U(\pi/gN_T)$ is what we denote W_t in the main text evaluated at some time t. The phase rotation with angle $\theta_a(t) = -\Omega(t)\pi/gN_T$ associated with the ancilla Hamiltonian does not affect the dynamics until $U(\pi/gN_T)^2$. The system-bath interaction yields an angle $\theta_i = 2\pi/N_T$. X_p is a probabilistic X gate, which is applied with probability $(1 - p_0(t))$, see text for details.

and develop a gate-based implementation of the time evolution. Crucial to the thermalization behavior is engineering the ancilla systems to mimic a macroscopic bath that is on average in a thermal state. To do this, we need to ensure that the ancilla qubits, whose local eigenbasis is the computational basis, are maintained in local thermal states over coarse timescales. We employ a (non-unitary) reset mechanism and a probabilistic application of a rotation in order to achieve this. The reset operation on all M ancilla qubits is defined as $\mathcal{R}\rho \equiv \sum_{i=0}^{2^M-1} |0\rangle\langle i|\,\rho\,|i\rangle\langle 0|$, where $|i\rangle$ is the M qubit state encoding the binary representation of i. In more detail, the state of the ancilla spin that we wish to maintain at a time t, is the (time-dependent) thermal state

$$\rho_b^{th}(t) = p_0(t)\,|0\rangle\langle 0| + (1 - p_0(t))\,|1\rangle\langle 1|\,, \tag{10}$$

$$p_0(t) = \frac{e^{\beta\Omega(t)/2}}{e^{\beta\Omega(t)/2} + e^{-\beta\Omega(t)/2}}. \tag{11}$$

We prepare this state by resetting the ancilla spin to $|0\rangle$ and applying a τ_x^m rotation with probability $(1 - p_0(t))$. The reset operations ensure the ancilla density matrix is diagonal and the dynamics are Markovian. An effective temperature is enforced through the Boltzmann distribution on the ancilla energy levels. The ancilla energies are resonant with the system energy transitions at different times, and after a full spectrum sweep the system is effectively coupled, on average, to a macroscopic bath at a fixed temperature [24]

Thermalization of the system relies on a separation of timescales between the system-bath interaction and the bath relaxation – essentially, the system should "see" all ancilla degrees of freedom in thermal states at the natural timescale of the system-bath interaction. Therefore, we distribute the ancilla reset and randomized preparation steps in such a way that there is a reset after a full cycle of system-ancilla interaction – i.e., after an evolution time $T_g = \pi/g$. From another perspective, weak coupling of the system to the ancilla and the periodic resets of the ancilla qubits ensure there is no correla-

tion between the ancilla spins, and phase differences will not lead to interference over the course of evolution. In order for effective thermalization of the system we require that the energy modulation of the ancilla be slower than the interaction timescale which is weak compared to the system interaction timescale. More precisely, we require the following hierarchy of parameters:

$$\left|\frac{df(t)}{dt}\right| \ll g \ll ||H_s||. \tag{12}$$

Conditions for heating and cooling of the system are determined by the average energy of the initial system

$$\langle E_s(t=0)\rangle = \mathrm{Tr}\left(\rho_s(t=0)H_s\right). \tag{13}$$

If the average energy is greater than (less than) the thermal energy $E_{th} = k_B T$, the system will cool (heat). We demonstrate in the numerical examination that system populations redistribute to thermal ensembles for random initial states.

Putting this together, the operation on the composite system for a period of system-ancilla interaction is,

$$\rho(t+T_g) = \left[\mathcal{I}\otimes\mathcal{R}\circ\mathcal{W}_t\circ\mathcal{I}\otimes\mathcal{X}_t\right]\rho(t), \tag{14}$$

where

$$\mathcal{W}_t\rho = W_t\rho W_t^\dagger, \quad \text{with} \quad W_t = \left[\left(\prod_{m=1}^{M} e^{-ig\left(\sigma_x^{\lambda(m)}\otimes\tau_x^m\right)\frac{T_g}{N_T}}\right)\left(e^{-iH_s\frac{T_g}{N_T}}\right)\left(\prod_{m=1}^{M}\left(e^{i\frac{\Omega(t)}{2}\tau_z^m\frac{T_g}{N_T}}\right)\right)\right]^{N_T}, \text{ and} \tag{15}$$

$$\mathcal{X}_t\rho = \otimes_{m=1}^{M}\left(p_0(t)\rho + (1-p_0(t))\tau_x^m\rho\tau_x^m\right). \tag{16}$$

Note that we have suppressed the identity operations on subsystems being acted on trivially. The operation $\mathcal{F}_t$ implements the probabilistic bit flip of the ancilla qubits. The order of the unitary operators in W_t describes the physical process of system-bath evolution, we first evolve by the system and bath Hamiltonians for a time T_g/N_T, followed by an application of the interaction. This is repeated for N_T iterations, where N_T is parameter to be chosen. Eq. 14 corresponds to a first-order Suzuki-Trotter discretization of the Hamiltonian dynamics described above coupled with the non-unitary operations of reset and probabilistic excitation of the ancilla qubits. The choice of N_T dictates the error incurred in discretizing the continuous coherent evolution by Hamiltonian in Eq. 1. To achieve an error of ϵ, we require $N_T = \mathcal{O}((3T_g\Lambda)^2/\epsilon)$ [31], where $\Lambda = \max(\|H_i\|, \|H_s\|, \|H_b\|)$. We note that one could implement the unitary portion of the dynamics, W_t, with higher order Suzuki-Trotter product formulas. This would increase the complexity of the gate sequence implementing the evolution but would allow for a smaller number of Trotter steps, N_T, while holding simulation error constant [32].

Eq. 14 provides a prescription for executing our thermalization algorithm on a quantum computer. A circuit representation of the sequence of operations is given in Figure 1(c). It is important to note that $\Omega(t)$, or more accurately $f(t)$, is assumed to be constant over an evolution time of T_g, consistent with the parameter hierarchy presented in Eq. 12. We introduce an additional parameter corresponding to the discretization of $f(t)$ – we assume one period of $f(t)$, T_{cycle} is divided into N_{cycle} steps of size T_g; i.e., $T_{\text{cycle}} = T_g \times N_{\text{cycle}}$ sets the timescale of the sweep of the ancilla energies. The overall dynamics over one T_{cycle} is then:

$$\rho(t+T_{\text{cycle}}) = \left[\prod_{k=0}^{N_{\text{cycle}}}\mathcal{R}\circ\mathcal{W}_t\circ\mathcal{X}_t\right]\left(\rho_s(t)\otimes|0\rangle_b\langle 0|\right), \tag{17}$$

with $t_k = kT_g$ and $|0\rangle_b\langle 0|$ denotes the state where all M ancilla qubits are in their ground state. Further, the state of the principal qubits after a period is

$$\begin{aligned}\rho_s(t+T_{\text{cycle}}) &\equiv \mathcal{M}_{cycle}\rho(t)\\ &= \mathrm{Tr}_b\left\{\left[\prod_{k=0}^{N_{\text{cycle}}}\mathcal{R}\circ\mathcal{W}_t\circ\mathcal{F}_t\right]\left(\rho_s(t)\otimes|0\rangle_b\langle 0|\right)\right\}.\end{aligned} \tag{18}$$

We have empirically determined that the parameter N_{cycle} scales as $\mathcal{O}\left(N_s/\min(\omega)\right)$ where $\min(\omega)$ is the smallest system transition frequency.

M_{cycle} describes the dynamics of the principal qubits after one sweep over the system energy spectrum. Several such sweeps are necessary in general to thermalize the principal system. The spectral gap, δ of the CPTP map $\mathcal{M}_{cycle}$ establishes an upper bound on the number of sweeps required to obtain a thermal distribution, *i.e.,* $N_{sweep} = \mathcal{O}\left(\beta N_s/\delta\right)$ [9, 33], and therefore ultimately determined the thermalization time.

IV. NUMERICAL EXAMINATION OF QMCMC

In this section we simulate our QMCMC algorithm on two model applications to determine its performance. The first is a paradigmatic spin model, the transverse-field Ising model (TFIM), and the goal is to prepare the thermal density matrix

Timescales and Estimates		
Interaction Evolution Time	T_g	$\frac{\pi}{g}$
Trotter Steps	N_T	$\mathcal{O}\left(\frac{(3T_g\Lambda)^2}{\epsilon}\right)$
Number of steps in a cycle	N_{cycle}	$\mathcal{O}\left(\frac{N_s}{\min(\omega)}\right)$
Sweep Period	T_{cycle}	$T_g \times N_{cycle}$
Number of sweeps	N_{sweep}	$\mathcal{O}\left(\frac{\beta N_s}{\delta}\right)$
Number of resets	$N_{\mathcal{R}}$	$\mathcal{O}\left(N_{sweep} \times N_{cycle}\right)$

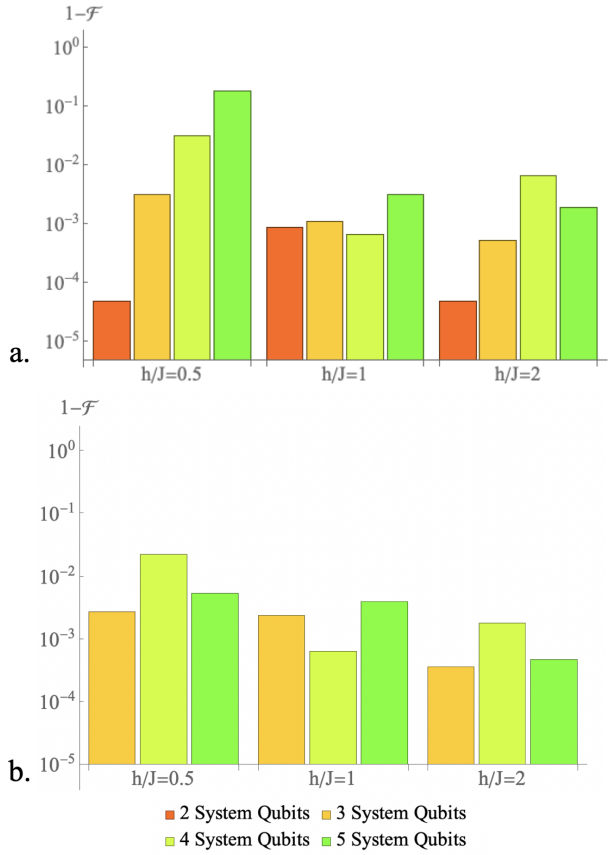

Figure 2. Infidelity of the QMCMC ground state with the genuine ground state for a) TFIM with open boundary conditions and b) TFIM with periodic boundary conditions. Each principal qubit is independently coupled bijectively to a single ancilla spin prepared – $\rho_b(0)$ – using $p_0 = 1$. The steady-state is obtained by diagonalizing the CPTP map $\mathcal{M}_{cycle}$.

of the model and reproduce thermal observables. The second example demonstrates our algorithm for the task of sampling from Gibbs distributions determined by probabilistic graphical models over classical random variables.

We determine the performance of our algorithm by numerically calculating the steady state of the dynamical map, $\mathcal{M}_{cycle}$, since the system dynamics is repeated application of this dynamical map and therefore the steady state of the system is the zero-eigenvalue eigenvector of the dynamical map

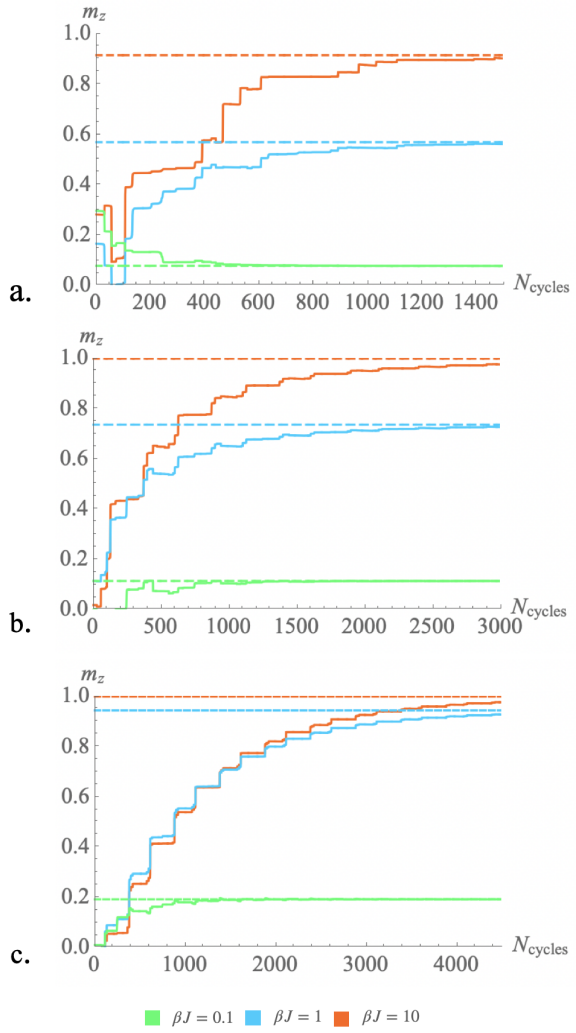

Figure 3. (upper) Time-evolved magnetization (solid) compared to exact thermal magnetization (dashed) of the TFIM with $N_s = 3$ at inverse temperature $\beta J = \{10, 1, 0.1\}$ for a) $h/J = 0.5$ with $N_{sweep} = 3$, b) $h/J = 1$ with $N_{sweep} = 6$, and c) $h/J = 2$ with $N_{sweep} = 9$. For each simulation the period of sweeping $T_{cycle} = 500T_g$ with $N_T = 5000$ Trotter steps. (Note: Horizontal axis ranges vary)

over T_{cycle}. In all of our numerical studies, $\mathcal{M}_{cycle}$ has a non-degenerate eigenspace at eigenvalue one, and thus a unique steady state. As discussed above, the inverse of the spectral gap of this map also determines the number of sweeps required to thermalize, and therefore thermalization timescale of a model [9].

Transverse Field Ising Model – The one-dimensional TFIM [34, 35] is defined by the Hamiltonian,

$$H = -J \sum_{i=1}^{N_s - 1} \sigma_z^i \sigma_z^{i+1} - h \sum_{i=1}^{N_s} \sigma_y^i, \tag{19}$$

which describes spins coupled locally with strength J in the presence of a transverse field h. Coupling strength J sets our

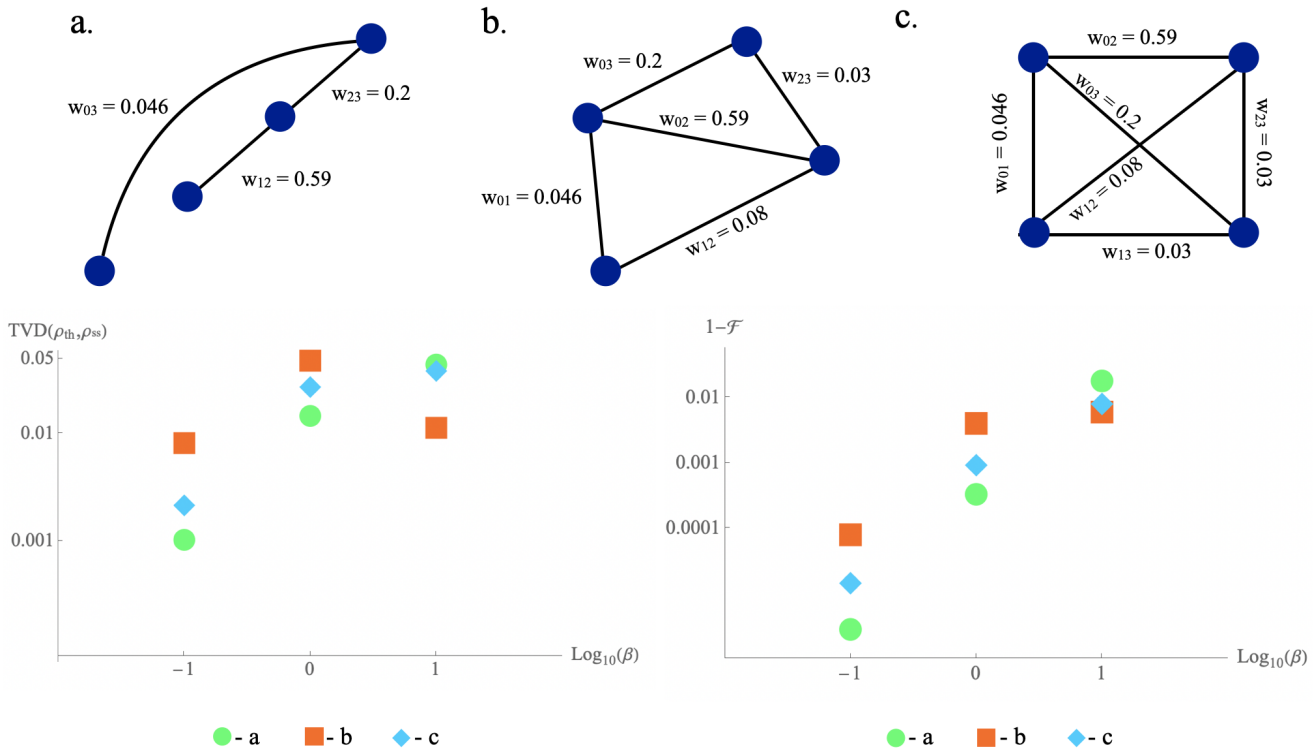

Figure 4. Total variational distance (TVD) and infidelity between the true Gibbs distribution and the distribution generated by the QMCMC algorithm for 3 random instances of graphs with 4 vertices and edge probability a) 0.4, b) 0.6, and c) 1 at inverse temperatures $\beta = 10, 1, 0.1$. The vertex values are $h_a = \{0.084, 0.026, 0.403, 0.379\}$, $h_b = \{0.403, 0.379, 0.0528, 0.805\}$, $h_c = \{0.379, 0.0528, 0.805, 0.379\}$ and are computed using the same seed as the edges.

energy and time scale for the Hamiltonian evolution. Each principal qubit is coupled to an ancillary qubit with an interaction strength $g/J = 0.005$ that sweeps the system spectrum with a sinusoidal $f(t) = \sin^2(\pi t/T_{\text{cycle}})$, with $N_T = 5000$ and $N_{\text{cycle}} \propto 10^2$, implying a period of $T_{\text{cycle}} = T_g N_{\text{cycle}} = 5\pi \times 10^4/J$.

To assess the quality of the thermalization, we compute the infidelity of the steady state of the dynamical map $\mathcal{M}_{cycle}$ defined above with the ideal thermal state at the simulation temperature. The infidelity is defined as $1 - \mathcal{F}$, with

$$\mathcal{F} = \text{Tr}\left(\sqrt{\sqrt{\rho_{th}}\rho_{ss}\sqrt{\rho_{th}}}\right)^2, \tag{20}$$

where ρ_{th} is the ideal thermal state, which for low temperatures approaches the ground state of the TFIM.

We benchmark the quality of our algorithm by examining ground state preparation in Fig. 2 for a) a TFIM with open-boundary conditions and b) TFIM with periodic boundary conditions with varying sizes and in three regimes: $h/J < 1$, $h/J = 1$, and $h/J > 1$. The target temperature for all simulations is $\beta J = 10$. Our algorithm performs well in generating ground states for both models including the periodic TFIM with degenerate energy sub-spaces. Our approximate thermal environment encoded on the ancilla spins exchanges energy with the symmetry sub-spaces and prepares the ground state of degenerate system Hamiltonians. At low fields energy transitions become similar requiring greater resolution of the sweeping function $f(t)$. We also find the greater resolution is needed for large system sizes with increased density of states. The steady-state error can improve in these regimes by increasing the resolution of the discrete ancilla sweeping function with N_{cycle} to approximate the continuum limit.

Finally, for this physically motivated example, we demonstrate the extraction of thermal observables after preparation of finite-temperature states with our algorithm. We evaluate the average magnetization $\langle m_z(t)\rangle = N_s^{-1}\text{Tr}\left(\rho_s(t)\sum_i^{N_s}\sigma_z^i\right)$ of a TFIM chain with $N_s = 3$ spins, show in Fig. 3. The system is prepared in a random initial state at time $t = 0$, and this random state is evolved in time using our method. The magnetization is evaluated after each iteration of the algorithm to show convergence to the exact, thermal expectation value. We examine this convergence in three transverse field regimes across a range of inverse temperatures βJ. The magnetization converged toward the thermal steady-state values for all of the test cases. We see more sweeping cycles are required for larger values of the transverse field. Convergence time to the steady-state distribution is inversely proportional to the gap of the CPTP map; therefore, the number of sweeping cycles needed scales inversely with the CPTP spectral gap. The spectral gap of the CPTP

map is smaller for larger fields, and our time-evolved results are in accordance with our CPTP map evaluations.

Sampling from Gibbs distributions – Sampling from Gibbs distributions of complex networks has a long history in statistical mechanics and machine learning [36–38]. MCMC techniques are the standard approach to such sampling problems, and here we demonstrate that our QMCMC algorithm can be used for such sampling problems.

Suppose we have a collection of binary random variables X_i, $1 \leq i \leq N_S$, whose configurations are dictated by a potential in the form of a quadratic formula in conjunctive normal form, $\eta(X_1,..N_{N_s})$. We are interested in sampling from the Gibbs distribution defined by $p(X_1,..N_{N_s}) = \exp(\eta(X_1,...X_{N_s}))/\mathcal{Z}$, where $\mathcal{Z} = \sum_{X_1,...X_{N_s}} \exp(\eta(X_1,...X_{N_s}))$ is a partition function. This is equivalent to sampling the Gibbs distribution over a probabilistic graphical model with nodes corresponding to the random variables and each edge corresponding to a clause in the potential formula [39].

We test the ability of QMCMC to prepare thermal states that enable such Gibbs sampling by encoding the potential in a Hamiltonian of the form

$$H_g = \sum_{i=1}^{N_s} h_i \sigma_z^i + \sum_{j,k\in\zeta} w_\zeta \sigma_z^j \sigma_z^k. \tag{21}$$

This Hamiltonian is equivalent to an encoding of $\eta(X_1,...X_{N_s})$, and the $|0\rangle, |1\rangle$ states of each qubit correspond to the possible values of the random variables. ζ lists all clauses in η. In the following, we generate random instances of such problems. To do so, we first generate Erdös-Rényi random graphs with edge probability p_e. These edges in this graph dictate ζ for the problem. Then for each edge we assign a weight, w_ζ, that is a random variable uniformly distributed in the interval $[0, 1]$, and for each variable we assign a random local energy, h_i, that is uniformly distributed in the interval $[0, 1]$.

After generating such a random instance and its corresponding Hamiltonian, we evaluate the ability of QMCMC to thermalize the many-body system by computing the steady state of the thermalization map $\mathcal{M}_{cycle}$, and comparing the distribution of measurement outcomes in the computational basis to the ideal Gibbs distribution $p(X_1,...X_{N_s})$. We use the total variation distance (TVD) to quantify the error between these distributions:

$$TVD(p,q) = \frac{1}{2} \sum_{i=0}^{2^{N_s}-1} |p_i - q_i| \tag{22}$$

In Fig. 4 we show the TVDs along with the infidelities achieved by QMCMC with a system-bath interaction strength of $g = 0.005$ for three random instances with varying p_e for several values of (inverse) temperature. We use the same sinusoidal $f(t)$ used in the TFIM calculations discretized by $N_{\text{cycle}} = 100$ and $N_T = 5000$. Distance between the true Gibbs distribution and distribution generated by sampling from the QMCMC steady-state is comparable to the infidelities seen for the TFIM example in the low temperature. Similar to the results for the TFIM, the trend observed in temperature for the physically motivated observable is a feature of the energy structure. Algorithmic accuracy depends on the system energy structure, and we can place no guarantees on the energy structure of a random instance. However, the *trend* seen by infidelity metric as a function of temperature is a good approximation for any given graph. These infidelity results are in good agreement with the analog protocol, accuracy increases with temperature.

V. CONCLUSION

Dynamically generating thermal states of quantum systems has historically required modeling a macroscopic environment or obtaining detailed knowledge of the system energy spectra, but in this work we demonstrate a method to represent these systems with linear spatial complexity using time-dependent, ancilla qubits. We analyzed the success of this model using magnetization as an observable in the TFIM and by numerically evaluating the fixed point of evolution for a random graph mapped to the Ising model. When the three criteria (Born-Markov, ergodic dynamics, and detailed balance energy exchange) are met, our algorithm generates a unique steady-state that approximates the thermal state. We aim to use this algorithmic framework to sample other complex distributions and define methods to generate non-equilibrium quantum distributions on quantum computers.

ACKNOWLEDGMENTS

AFK and ES were supported by the Department of Energy, Office of Basic Energy Sciences, Division of Materials Sciences and Engineering under Grant No. DE-SC001946. WAdJ, MM, and KK were supported by the U.S. Department of Energy (DOE) under Contract No. DE-AC02-05CH11231, through the Office of Advanced Scientific Computing Research Accelerated Research for Quantum Computing and Quantum Algorithms Team Programs. MS was supported by the U.S. Department of Energy, Office of Science, Office of Advanced Scientific Computing Research, under the Quantum Computing Application Teams program.

Sandia National Laboratories is a multimission laboratory managed and operated by National Technology & Engineering Solutions of Sandia, LLC, a wholly owned subsidiary of Honeywell International Inc., for the U.S. Department of Energy's National Nuclear Security Administration under contract DE-NA0003525. This paper describes objective technical results and analysis. Any subjective views or opinions that might be expressed in the paper do not necessarily represent the views of the U.S. Department of Energy or the United States Government.

[1] D. Bacon, A. M. Childs, I. L. Chuang, J. Kempe, D. W. Leung, and X. Zhou, "Universal simulation of markovian quantum dynamics," Phys. Rev. A **64**, 062302 (2001).

[2] R. Di Candia, J. S. Pedernales, A. del Campo, E. Solano, and J. Casanova, "Quantum simulation of dissipative processes without reservoir engineering," Sci. Rep. **5**, 9981 (2015).

[3] H.Y. Su and Y. Li, "Quantum algorithm for the simulation of open-system dynamics and thermalization," Phys. Rev. A **101**, 012328 (2020).

[4] R. Sweke, M. Sanz, I. Sinayskiy, F. Petruccione, and E. Solano, "Digital quantum simulation of many-body non-markovian dynamics," Phys. Rev. A **94**, 022317 (2016).

[5] Chenu M., Beau J., Cao, and A. del Campo, "Quantum simulation of generic many-body open system dynamics using classical noise," Phys. Rev. Lett. **118**, 140403 (2017).

[6] Kade Head-Marsden, Stefan Krastanov, David A. Mazziotti, and Prineha Narang, "Capturing non-markovian dynamics on near-term quantum computers," Phys. Rev. Research **3**, 013182 (2021).

[7] Richard Cleve and Chunhao Wang, "Efficient quantum algorithms for simulating lindblad evolution," (2016), arXiv:1612.09512 [quant-ph].

[8] Andrew M. Childs and Tongyang Li, "Efficient simulation of sparse Markovian quantum dynamics," 10.26421/QIC17.11-12, arXiv:1611.05543v2 [quant-ph].

[9] K Temme, T J Osborne, K G Vollbrecht, and D Poulin, "Quantum metropolis sampling," Nature **471**, 87–90 (2011).

[10] Man-Hong Yung and Alán Aspuru-Guzik, "A quantum–quantum metropolis algorithm," Proceedings of the National Academy of Sciences **109**, 754–759 (2012).

[11] Mario Szegedy, "Quantum speed-up of markov chain based algorithms," in *45th Annual IEEE symposium on foundations of computer science* (IEEE, 2004) pp. 32–41.

[12] Pawel Wocjan and Anura Abeyesinghe, "Speedup via quantum sampling," Physical Review A **78**, 042336 (2008).

[13] Dominik S Wild, Dries Sels, Hannes Pichler, and Mikhail D Lukin, "Quantum sampling algorithms for near-term devices," arXiv preprint arXiv:2005.14059 (2020).

[14] Guillaume Verdon, Jacob Marks, Sasha Nanda, Stefan Leichenauer, and Jack Hidary, "Quantum hamiltonian-based models and the variational quantum thermalizer algorithm," arXiv:1910.02071 (2019).

[15] Suguru Endo, Jinzhao Sun, Ying Li, Simon C Benjamin, and Xiao Yuan, "Variational quantum simulation of general processes," Physical Review Letters **125**, 010501 (2020).

[16] D. Zhu, S. Johri, N. M. Linke, K. A. Landsman, C. Huerta Alderete, N. H. Nguyen, A. Y. Matsuura, T. H. Hsieh, and C. Monroe, "Generation of thermofield double states and critical ground states with a quantum computer," PNAS **117**, 25402–25406; (2020).

[17] Akhil Francis, D. Zhu, C. Huerta Alderete, Sonika Johri, Xiao Xiao, J. K. Freericks, C. Monroe, N. M. Linke, and A. F. Kemper, "Many body thermodynamics on quantum computers via partition function zeros," ArXiv , 2009.04648 (2020).

[18] Steven R White, "Minimally entangled typical quantum states at finite temperature," Physical review letters **102**, 190601 (2009).

[19] EM Stoudenmire and Steven R White, "Minimally entangled typical thermal state algorithms," New Journal of Physics **12**, 055026 (2010).

[20] Mario Motta, Chong Sun, Adrian T. K. Tan, Matthew J. O'Rourke, Erika Ye, Austin J. Minnich, Fernando G. S. L. Brandão, and Garnet Kin-Lic Chan, "Determining eigenstates and thermal states on a quantum computer using quantum imaginary time evolution," Nature Physics **16**, 205–210 (2020).

[21] Shi-Ning Sun, Mario Motta, Ruslan N. Tazhigulov, Adrian T. K. Tan, Garnet Kin-Lic Chan, and Austin J. Minnich, "Quantum computation of finite-temperature static and dynamical properties of spin systems using quantum imaginary time evolution," arXiv:2009.03542 (2020).

[22] H-P Breuer and F Petruccione, *The theory of open quantum systems*, Book (Springer, 2002).

[23] Alireza Shabani and Hartmut Neven, "Artificial quantum thermal bath: Engineering temperature for a many-body quantum system," Phys. Rev. A **94**, 052301 (2016).

[24] Mekena Metcalf, Jonathan E Moussa, Wibe A de Jong, and Mohan Sarovar, "Engineered thermalization and cooling of quantum many-body systems," Physical Review Research **2**, 023214 (2020).

[25] David A Levin and Yuval Peres, *Markov chains and mixing times*, Vol. 107 (American Mathematical Soc., 2017).

[26] Ashley Montanaro, "Quantum speedup of monte carlo methods," Proceedings of the Royal Society A: Mathematical, Physical and Engineering Sciences **471**, 20150301 (2015).

[27] Vera von Burg, Guang Hao Low, Thomas Häner, Damian S Steiger, Markus Reiher, Martin Roetteler, and Matthias Troyer, "Quantum computing enhanced computational catalysis," arXiv preprint arXiv:2007.14460 (2020).

[28] David B. Kaplan, Natalie Klco, and Alessandro Roggero, "Ground states via spectral combing on a quantum computer," arXiv:1709.08250 (2017).

[29] Stefano Polla, Yaroslav Herasymenko, and Thomas E O'Brien, "Quantum digital cooling," arXiv preprint arXiv:1909.10538 (2019).

[30] Stefano Polla, Yaroslav Herasymenko, and Thomas E. O'Brien, "Quantum digital cooling," Phys. Rev. A **104**, 012414 (2021).

[31] Andrew M Childs, Aaron Ostrander, and Yuan Su, "Faster quantum simulation by randomization," Quantum **3**, 182 (2019).

[32] Andrew M. Childs, Yuan Su, Minh C. Tran, Nathan Wiebe, and Shuchen Zhu, "A Theory of Trotter Error," Phys. Rev. X **11**, 011020 (2021).

[33] Kristan Temme, "Lower bounds to the spectral gap of davies generators," J. Math. Phys. **54**, 122110 (2013).

[34] PG De Gennes, "Collective motions of hydrogen bonds," Solid State Communications **1**, 132–137 (1963).

[35] RB Stinchcombe, "Ising model in a transverse field. i. basic theory," Journal of Physics C: Solid State Physics **6**, 2459 (1973).

[36] Iain Murray and Zoubin Ghahramani, "Bayesian learning in undirected graphical models: approximate mcmc algorithms," Proceedings of the 20th conference on Uncertainty in artificial intelligence , 392–399 (2004).

[37] B.J. Frey and N. Jojic, "A comparison of algorithms for inference and learning in probabilistic graphical models," IEEE Transactions on Pattern Analysis and Machine Intelligence **27**, 1392 – 1416 (2005).

[38] Réka Albert and Albert-László Barabási, "Statistical mechanics of complex networks," Rev. Mod. Phys. **74** (2002).

[39] D. Koller and N. Friedman, *Probabilistic Graphical Models: Principles and Techniques*, Adaptive computation and machine learning (MIT Press, 2009).